



# Alanine to serine substitutions drive thermal adaptation in a psychrophilic diatom cytochrome $c_6$

Miranda Wilson<sup>1</sup> · Logan Tillery<sup>1</sup> · Emily Tabaie<sup>1</sup> · Galen Beery<sup>1</sup> · Jordyn Preusker<sup>1</sup> · Inaara Bhola<sup>1</sup> · Katherine Frato<sup>1</sup>

Received: 3 October 2019 / Accepted: 16 March 2020 / Published online: 27 March 2020  
© Society for Biological Inorganic Chemistry (SBIC) 2020

**Keywords** Psychrophile · Cytochrome  $c_6$  · Mesophile · Thermal denaturation ·  $m$ -value · Electrochemistry · Site-directed mutagenesis

## Abbreviations

cyt $c$	Cytochrome $c$
Fc	<i>Fragilariopsis cylindrus</i>
Tp	<i>Thalassiosira pseudonana</i>
PGE	Pyrolytic graphite edge
Gdn	Guanidine HCl
$E_{\text{mid}}$	Midpoint potential

## Introduction

Life has evolved in a wide range of thermal environments, from polar ice to volcanic hot springs. Protein function at any temperature requires a balance of stability and conformational flexibility. Tertiary structures must be sufficiently stable to favor the folded structure or ensemble, yet flexible enough to allow conformational changes required for function. Cold environments provide less of the thermal energy that drives the dynamic motion of folded proteins. Therefore, proteins that are adapted to function at temperatures around or below the freezing point of water must have more conformational flexibility, and presumably be less stable, in order to maintain function.

Enzymes from psychrophiles have demonstrated that a range of sequence adaptations are used to optimize activity in environments with less thermal energy. Some general trends found in psychrophilic enzymes to increase structural

flexibility include: over-representation of glycine residues, under-representation of proline residues, fewer hydrogen bonds, fewer surface ion-pairs, fewer arginine residues, more exposed hydrophobic surface area, and less-compact hydrophobic cores [1–3]. It appears that each protein family or fold uses a different combination of these strategies to adapt to cold temperatures [3].

When compared to enzymes, electron transfer proteins have a slightly different set of functional constraints. Unlike enzymes, electron transfer proteins such as  $c$ -type cytochromes should be relatively rigid to optimize electron transfer rates. Marcus theory states that the rate of the electron transfer should be faster for systems with lower reorganization energy, which can be minimized by limiting the change in the location of nuclei between the oxidized and reduced states [4]. However, electron transfer proteins must have small differences in the shape and charge distribution between oxidation states to perturb the binding affinity between donor and acceptor proteins and facilitate unbinding following electron transfer. Members of the cytochrome  $c_6$  family have been shown to be quite rigid; no redox dependent conformational change was observed when comparing crystal structures of the oxidized and reduced forms of cytochrome  $c_6$  from the green alga *Scenedesmus obliquus* [5, 6]. In  $c$ -type cytochromes, redox dependent changes must involve relatively subtle reorganization of side chains or changes in residue mobility.

A second aspect of electron transfer proteins that must adapt to environmental temperature is the reduction potential of the electroactive group. The driving force for electron transfer is derived from the relative reduction potentials of the electron donor and acceptor groups. Midpoint potentials vary with temperature, and the magnitude of the change depends on the change in entropy for the reduction process,  $\Delta S_{\text{rc}}^{\circ}$ . For  $c$ -type cytochromes,  $\Delta S_{\text{rc}}^{\circ}$  is always large and negative, but differs in magnitude [7, 8]. Therefore,  $c$ -type

**Electronic supplementary material** The online version of this article (<https://doi.org/10.1007/s00775-020-01777-0>) contains supplementary material, which is available to authorized users.

✉ Katherine Frato  
fratok@seattleu.edu

<sup>1</sup> Department of Chemistry, Seattle University, 901 12th Ave., Seattle, WA 98122, USA

cytochromes adapted to function at differing temperatures may modulate both midpoint potential and folding stability to maintain function.

The cytochrome *c* family is widespread throughout the tree of life and serves a variety of electron transport functions, including required roles in oxidative phosphorylation and photosynthesis. Cytochrome *c*<sub>6</sub> is a small, soluble protein with a His-Met ligated *c*-type heme that mediates the transfer of electrons between the membrane-embedded cytochrome *b*<sub>6</sub>*f* complex and photosystem I. We identified, based on amino acid sequence similarity, putative cytochrome *c*<sub>6</sub> sequences in the published genome sequences of the mesophilic diatom *Thalassiosira pseudonana* [9] and the psychrophilic diatom *Fragilariopsis cylindrus* [10]. *Thalassiosira pseudonana* is a cosmopolitan diatom capable of growth at a wide range of environmental temperatures, with highest growth rates between 20–30 °C [11–13]. *Fragilariopsis cylindrus* demonstrates growth and photosynthesis at temperatures as low as –1 °C [14–16]. A multiple sequence alignment comparing canonical cytochrome *c*<sub>6</sub> family members to the putative *Fc* and *Tp* cyt *c*<sub>6</sub> sequences supports their functional assignment as photosynthetic electron transfer proteins (Supplementary Figure S1). The presence of bipartite signal peptides with a conserved “ASAF” motif in both sequences further supports chloroplast localization [17, 18].

The putative cytochrome *c*<sub>6</sub> proteins from *F. cylindrus* and *T. pseudonana* are 90% identical, considering only the mature sequences with presumed signal peptides removed (Fig. 1). Since primary sequence defines three-dimensional structure and function, any difference in the thermal adaptation of the two proteins must be accounted for by the few amino acid differences. Of the differences, four are highly conservative aspartate versus glutamate, and another two are also conservative differences which maintain polar and hydrogen bonding character (serine/asparagine and serine/threonine). Four locations demonstrate shifts in polar vs. nonpolar character (serine/alanine), and are most likely to impact function. Serine and alanine share very similar codons; in fact, a G to T mutation in the first nucleotide of any alanine codon converts it to a serine codon. Another intriguing difference is the single, additional acidic residue appended to the C-terminus of the *F. cylindrus* sequence.

In this study, we investigate the interplay between the thermodynamic stability of a protein fold and the heme reduction potential through the direct comparison of a psychrophilic cytochrome *c* and a highly homologous mesophilic control. Direct voltammetry is used to measure the reduction potentials and support assignment of the proteins to the cytochrome *c*<sub>6</sub> family. The variation of reduction potential with temperature allows us to extract the change in entropy and enthalpy of the reduction

process for the two proteins. Through analysis of thermal and chemical denaturation of the two homologous *c*-type cytochromes we identify key folding parameters that differ between the two proteins. Comparison of the wild-type proteins, as well as the melting temperature of alanine to serine mutants, reveals the role of specific residues in thermal adaptation. Based on our results, we hypothesize that differences between the solvation of the folded state of the homologs result in lower stability of the psychrophilic protein, which may facilitate activity at lower environmental temperatures.

## Materials and methods

### Chemicals

All reagents were BioReagents grade from Fisher Scientific (Waltham, MA) unless otherwise specified.

### Construction of plasmid for recombinant overexpression of wild-type and variant cyt *c*<sub>6</sub>

Complete predicted amino acid sequences for *Fc* cyt *c*<sub>6</sub> and *Tp* cyt *c*<sub>6</sub> were obtained from the Joint Genome Institute Genome Browser [19]. Signal peptide sequences were identified by analogy to other known diatom plastid signal sequences using online web servers SignalP [20] and ASA-Find [18]. Nucleotide sequences corresponding to only the mature polypeptides were codon optimized for expression in *Escherichia coli* and synthesized as GeneArt strings (Life Technologies, Carlsbad, CA). Empty pET22b(+) plasmid (Millipore Sigma, Burlington, MA) was linearized by sequential restriction digest with BamHI and HindIII, and purified using GeneJET Gel Extraction and DNA Cleanup Micro Kit (Thermo Scientific, Waltham, MA). *Fc*271949 or *Tp*35934 coding sequences were inserted into linearized plasmid using Gibson Assembly Master Mix according to the manufacturer's standard protocol (New England Biolabs, Ipswich, MA). Constructs with N-terminal pelB periplasmic localization sequences, pET22b-*Fc*271949 and pET22b-*Tp*35934, were confirmed by gene sequencing (Genewiz, South Plainfield, NJ).

*Tp*35934 single site variants A86S, A93S, and A126S were constructed using QuikChange Lightning Site-Directed Mutagenesis Kit (Agilent, Santa Clara, CA). Mutation positions were numbered based on the full open reading frame of *Tp*35934 in the *T. pseudonana* genome. Primers sequences are given in the supporting information (Table S1). The double mutant *Tp*35934 A93S/A126S was generated from the A93S parent using *Tp*35934-A126S-F and *Tp*35934-A126S-R primers.

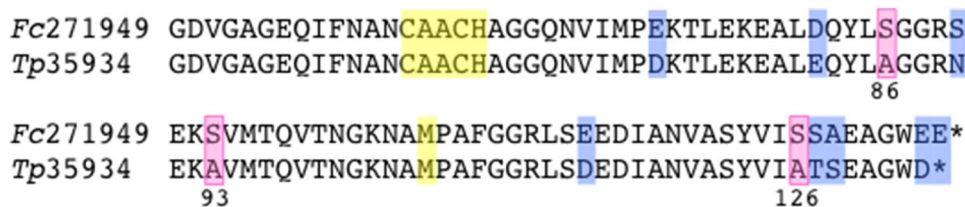


**Fig. 1** Amino acid sequence alignment for mature versions of cytochrome  $c_6$  proteins from *Fragilariopsis cylindrus* (Fc271949) and *Thalassiosira pseudonana* (Tp35934), with presumed signal peptide sequences removed. Yellow highlighting indicates key  $c$ -type heme

attachment sites and axial ligands. Blue and pink highlighting indicate amino acid positions that differ between homologs. Pink positions are serine in Fc271949 but alanine in Tp35934, and are numbered to match the description in the text

## Expression and purification of $c$ -type cytochromes

Plasmids carrying wild-type Fc271949, Tp35934, and Tp35934 variants were each transformed into chemically competent *E. coli* BL21(DE3) carrying the pEC86 plasmid [21]. Transformed cells were selected on LB agar (100  $\mu$ g/mL ampicillin, 15  $\mu$ g/mL chloramphenicol). Single colonies were inoculated into 5 mL LB media (100  $\mu$ g/mL ampicillin, 15  $\mu$ g/mL chloramphenicol) and grown overnight at 37 °C. Overnight cultures were centrifuged to pellet, resuspended in fresh LB media, and the equivalent of 2.5 mL of overnight culture was used to inoculate each 0.5 L of 2xYT media (Research Products International, Mount Prospect, IL). Cultures were incubated with vigorous shaking until mid-log phase ( $OD_{600}=0.6-0.8$ ), and expression was induced using 0.3 mM final concentration of  $\beta$ -D-1-thiogalactopyranoside (IPTG, Sigma-Aldrich, St. Louis, MO). Cultures were grown for an additional 3 h at 80 rpm and 37 °C. Bacteria were collected via centrifugation and resuspended in a minimal volume of buffer A (20 mM Tris pH 8.0) before storage in  $-80$  °C.

The thawed cell pellet was resuspended in 80 mL of buffer A for each 1 L of bacterial culture. Lysis was initiated by addition of 0.04% (w/v) final concentration of sodium deoxycholate, 0.1 mM final concentration of phenylmethylsulfonyl fluoride (PMSF) and approximately 2 mg lysozyme per 80 mL lysate and allowed to proceed on ice for 15 min. Following incubation for an additional 30 min in the presence of approximately 2 mg of DNase I (Sigma-Aldrich, St. Louis, MO) per 80 mL lysate, the insoluble fraction was removed via centrifugation at 4 °C and 11627 $\times g$  (maximum RCF). All chromatography steps were controlled using Akta Start FPLC system (GE Healthcare, Marlborough, MA). Clarified lysate was separated by HiTrap DEAE FF (5 mL, GE Healthcare, Marlborough, MA) equilibrated in buffer A and eluted in a gradient of 0–50% of buffer B (20 mM Tris pH 8.0, 1 M NaCl). Fractions were screened for purity and accurate folding by absorbance spectroscopy, and fractions with  $A_{416nm}/A_{280nm} > 1$  and a sharp Soret band at 416 nm were combined and concentrated using Amicon Ultra-15 10 K molecular weight cut-off centrifugal concentrator units

(Millipore Sigma, Burlington, MA). Concentrated samples were loaded onto a HiPrep 16/60 Sephacryl S-200 h gel filtration column (GE Healthcare, Marlborough, MA) equilibrated with 20 mM Tris, 150 mM NaCl pH 8.0 at 0.5 mL/min. Fractions with high purity of cytochrome  $c$  as determined by  $A_{416nm}/A_{280nm}$  greater than 4 were combined and concentrated as before. Purified protein samples were stored in 15% glycerol at  $-80$  °C until use. Extinction coefficients were determined by pyridine heme assay [22].

## Cyclic voltammetry of protein solutions

Cyclic voltammograms were collected using a modified membrane electrode setup. Edge plane pyrolytic graphite (3.0 mm diameter) or gold (1.6 mm diameter) working electrode, Ag/AgCl (3 M NaCl) reference electrode, and platinum wire counter electrode were all purchased from BASi (West Lafayette, IN). Graphite working electrode was polished with sandpaper, followed by 0.05  $\mu$ m particle size alumina. Gold electrode surfaces were polished mechanically with diamond suspension, then cleaned electrochemically by cycling in a cell solution of 1 M sulfuric acid between  $-0.2$  V and  $+1.6$  V versus Ag/AgCl for at least ten cycles. Cleaned electrodes were immersed in ethanolic solutions of either 4 mM mercaptoethanol or mercaptohexanol and incubated overnight. To assemble the membrane electrode, 2  $\mu$ L of concentrated protein (100–300  $\mu$ M) was pipetted directly onto the cleaned graphite surface, then a small square of moistened SnakeSkin 10 kDa MWCO dialysis membrane (Thermo Scientific, Waltham, MA) was secured over the electrode end with an O-ring. Experiments were controlled using BASi EC Epsilon Potentiostat with Epsilon EC v.2.13.77 software. Temperature was controlled using a water jacketed cell with circulating water bath. The temperature inside the electrochemical cell was independently monitored immediately before and after each scan. Voltammograms were analyzed using QSOAS [23]. Errors in  $\Delta H^\circ_{rc}$  and  $\Delta S^\circ_{rc}$  are calculated from the standard deviations of three independent experiments monitoring the effect of temperature on midpoint potential.

## Thermal denaturation

Absorption spectra were collected from 350–800 nm over increasing temperature using Agilent Cary 100 Spectrophotometer (Santa Clara, CA) with Quantum Northwest t2×2 Sport temperature-controlled sample holder (Liberty Lake, WA). Each experiment contained between 3–7 μM final concentration of cyt  $c_6$  in 50 mM 4-(2-hydroxyethyl)piperazine-1-ethanesulfonic acid (HEPES) pH 7.4. Temperature was increased by 2 °C increments from 18–49 °C (Fc cyt  $c_6$ ) or 24–60 °C (Tp cyt  $c_6$ ) with 3.5 min equilibration time between each temperature increase. Samples were supplemented with stoichiometric amounts of potassium ferricyanide to oxidize, and oxygen was excluded with a continuous nitrogen purge in the headspace. Reversibility was tested by returning each sample back to the initial temperature following the complete thermal denaturation experiment, and spectra were collected following at least 10 min of equilibration at low temperature.

Melting temperatures ( $T_m$ ) and van't Hoff enthalpies ( $\Delta H_{vH}$ ) were determined by fitting the thermal denaturation data at 403 nm using a derivative form of the van't Hoff equation [24]. Tabulated values reported are averages from three independent experiments.

## Chemical denaturation

Free energy changes upon unfolding were determined by chemical denaturation and monitored by absorption spectroscopy using Agilent Cary 100 Spectrophotometer (Santa Clara, CA) with Quantum Northwest t2×2 Sport temperature-controlled sample holder (Liberty Lake, WA). Stock solutions of 5 μM cytochrome  $c$  in 50 mM HEPES pH 7.4 and either 0 M and 6 M guanidine HCl were mixed in various ratios to generate intermediate denaturant concentrations in 150 μL final volume. Mixtures of 0 M and 6 M guanidine HCl stock solutions tested in the absence of protein showed a pH variance within 0.1 pH unit. The concentration of guanidine HCl stocks were determined by the mass of solid added and total volume. An oxidizing environment was maintained throughout the experiment by 28 μM final concentration of potassium ferricyanide. Samples were incubated for 2 h at 15 °C, spectra were collected from 350–800 nm, and baselines were renormalized to correct for instrument drift. Unfolding was monitored as the change in absorbance at 403 nm. Plots of absorbance (Abs) versus concentration of guanidine HCl ([Gdn]) were fit to a standard two-state model using the linear extrapolation method [25, 26]:

$$\text{Abs} = \frac{(\text{Abs}_N) + \text{Abs}_D e^{-\left(\frac{\Delta G_{N-D} - m[\text{Gdn}]}{RT}\right)}}{1 + e^{-\left(\frac{\Delta G_{N-D} - m[\text{Gdn}]}{RT}\right)}}$$

where  $\text{Abs}_N$  and  $\text{Abs}_D$  are the absorbance of the native and denatured population at the monitored wavelength,  $m$  is the slope of the unfolding transition (the  $m$ -value),  $\Delta G_{N-D}$  is the free energy of unfolding at 0 M guanidine HCl, and RT is calculated at 15 °C. Fits were conducted on data averaged from three independent replicates using three independent preparations of the HEPES-buffered 6 M guanidine HCl stock solution. The same three 6 M guanidine HCl stock solutions were used for both Tp and Fc cyt  $c_6$  unfolding experiments to control comparative data against error in guanidine stock concentrations.

## Results

### Recombinant expression and purification of diatom cytochrome $c_6$

Putative cytochrome  $c_6$  from *F. cylindrus* and *T. pseudonana* were recombinantly expressed in *E. coli* in a soluble conformation with high fractional loading of heme. Following ion exchange and size-exclusion chromatography, protein stocks routinely showed purity indices ( $A_{416\text{nm}}/A_{280\text{nm}}$ ) of  $> 5$ , suggesting a high ratio of heme-containing cytochrome relative to non-heme protein contaminants. Both  $c$ -type cytochromes were expressed and purified in the reduced state, with Soret band at 416 nm and  $Q$  band features at 522 nm and 553 nm. Protein stocks remained mostly reduced even after extended storage in oxygenated buffer, suggesting a relatively high reduction potential. Upon oxidation with potassium ferricyanide,  $Q$  bands broaden and the Soret band shifts to 408.5 nm. Extinction coefficients for the reduced, native state at 553 nm as determined by pyridine heme assay were  $24.2 \pm 1.4 \text{ mM}^{-1} \text{ cm}^{-1}$  for Tp cyt  $c_6$  and  $27 \pm 2 \text{ mM}^{-1} \text{ cm}^{-1}$  for Fc cyt  $c_6$ . Pyridine heme spectra were consistent with a  $c$ -type heme attachment (data not shown).

### Midpoint reduction potential

The midpoint potentials of wild-type Fc and Tp cyt  $c_6$  were determined using cyclic voltammetry. Proteins failed to adsorb to pyrolytic graphite edge or SAM-modified gold surfaces in a mode competent for electron transfer. Therefore, measurements were conducted using a membrane electrode setup, where a small volume of concentrated protein solution is sequestered in a thin film near the electrode surface using piece of dialysis membrane [27]. Using the membrane electrode setup, we observe reversible electron transfer on graphite, or mercaptoethanol or mercaptohexanol SAM-modified gold electrodes (Fig. 2). It has been previously shown that the membrane electrode setup sequesters a layer of protein approximately 10 μm thick near the electrode, and at scan

rates below 100 mV/s the film is sufficiently thin that mass transfer effects can be neglected [27, 28].

Characteristics of the voltammograms measured at low scan rates confirm that the thin protein layer behaves according to a thin-layer model. The peak separation between the oxidative and reductive peaks varied between 10–40 mV at 2 mV/s scan rate, and were generally smaller when passivated gold electrodes were used. The observed values for peak separation were less than the minimal theoretical peak separation of 52 mV expected for a diffusion-controlled system at 0 °C. Peak widths at half-height were approximately 90 mV at 2 mV/s, similar to the expected 83 mV peak width expected for a thin-layer model. Plots of peak current versus scan rate demonstrate a linear relationship at low scan rates, also consistent with a thin-layer model (Supplementary Figure S2). Therefore, electrochemical data are analyzed using a thin-layer model.

The midpoint potentials for *Fc* and *Tp* cyt  $c_6$  proteins were determined using cyclic voltammetry (Table 1). A single oxidative and reductive wave were observed on either graphite or gold electrodes, indicating only one electroactive group was being monitored. Peak potentials were consistent over varying electrode surfaces; for *Tp* cyt  $c_6$ , the  $E_{\text{mid}}$  on mercaptohexanol-modified gold was 382 mV vs. SHE, whereas the  $E_{\text{mid}}$  on graphite was 387 mV vs. SHE. We did not observe any low-potential “Met-loss” forms often observed in His-Met ligated *c*-type cytochromes proteins adsorbed directly to graphite surfaces [29, 30]. We observe a slight difference in the midpoint potentials between the *Fc* and *Tp* cyt  $c_6$  proteins, with the mesophilic *Tp* cyt  $c_6$  displaying a midpoint potential approximate 4 mV higher than the psychrophile *Fc* cyt  $c_6$  at 0 °C and 15 °C.

Changes in enthalpy ( $\Delta H_{\text{rc}}^{\circ}$ ) and entropy ( $\Delta S_{\text{rc}}^{\circ}$ ) for the reduction process were calculated by monitoring the change

in midpoint potential with temperature (Fig. 1c, Table 1). Qualitatively, the curve for *Tp* cyt  $c_6$  is shifted up in potential relative to *Fc* cyt  $c_6$ . While the slopes are very similar over the 30 °C range monitored, the slope for the *Fc* cyt  $c_6$  plot is slightly steeper than the slope of the *Tp* cyt  $c_6$  plot. The entropy change is determined as the slope of the midpoint potential vs. temperature plot and the enthalpy change is the slope of the  $E/T$  versus  $T$  (Gibbs–Helmholtz) plot. Corresponding values for  $\Delta H_{\text{rc}}^{\circ}$  and  $\Delta S_{\text{rc}}^{\circ}$  for the two homologs are essentially the same.

## Thermal unfolding

Thermal unfolding was monitored from the oxidized, native state (Fig. 3). As temperature increases, the absorption spectrum shifts without observable intermediates to an oxidized, denatured state that has a Soret band at 404 nm, slightly increased Soret intensity and slightly decreased Q-band intensity. A minor feature at 630 nm builds in as the protein unfolds, suggesting the formation of a high-spin pentacoordinate state upon unfolding [31]. For all thermal unfolding experiments, reversibility was tested by returning the system to the starting temperature, allowing 10 min of temperature equilibration; experiments showed > 90% return to the oxidized, native state (Supplementary Figure S3). Thermal unfolding monitored by intrinsic tryptophan fluorescence similarly shows a single unfolding transition and melting temperature consistent with those observed using absorption spectroscopy, confirming that the proteins unfold cooperatively (Supplementary Figure S4).

To extract melting temperature and van't Hoff enthalpy values, thermal denaturation data were analyzed at a single wavelength. Derivative plots were calculated and fit according to a modified van't Hoff equation [24]. Representative

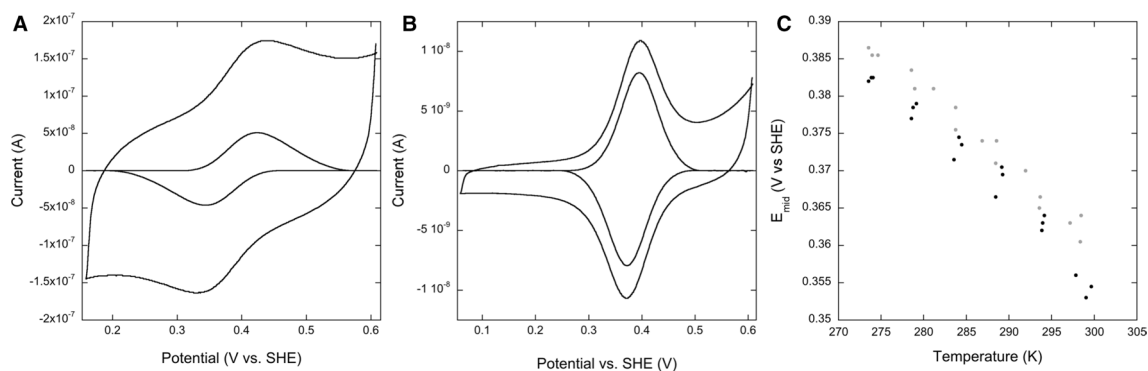


**Fig. 2** Cyclic voltammetry of cytochrome  $c_6$  **a** Raw voltammogram and baseline-subtracted data for *Fc* cyt  $c_6$  collected at 0.3 °C in 20 mM HEPES, 1 M NaCl pH 7.5; edge plane pyrolytic graphite electrode, scan rate 2 mV/s **b** Raw voltammogram and baseline-subtracted data for *Tp* cyt  $c_6$  collected at 0.2 °C, mercaptoethanol passivated gold electrode, scan rate 2 mV/s. **c** Relationship between mid-

point potential ( $E_{\text{mid}}$ ) and temperature for *Fc* cyt  $c_6$  (black) and *Tp* cyt  $c_6$  (gray) showing data from three independent trials. Midpoint potentials were determined as the average of oxidative and reductive peak potentials. Experimental buffer is 20 mM HEPES, 300 mM NaCl, pH 7.5, and data are collected at a scan rate of 2 mV/s

derivative data with fits are shown in Fig. 4a. The psychrophilic cytochrome *Fc* cyt  $c_6$  melts at a significantly lower temperature than the mesophilic cytochrome *Tp* cyt  $c_6$ .

Melting experiments were completed in triplicate and results from independent fits were averaged to give the data presented in Table 2. The oxidized psychrophilic protein melts at a temperature 10.4 °C lower than the oxidized mesophilic protein. The van't Hoff enthalpy change upon unfolding for *Fc* cyt  $c_6$  and *Tp* cyt  $c_6$  do not show significant differences.

### Guanidine unfolding experiments

UV–Vis spectrophotometry was used to monitor the fraction of the folded state for cytochrome  $c_6$  over increasing concentrations of the chemical denaturant guanidine hydrochloride. Free energy changes were measured at 15 °C because the oxidized form of *Fc* cyt  $c_6$  showed a substantial population in the unfolded state at ambient lab temperature. Spectral changes during chemical denaturation mirrored the changes observed for the folded to unfolded transition in thermal denaturation. Figure 4b demonstrates the normalized average of three independent trials for each of *Fc* cyt  $c_6$  or *Tp* cyt  $c_6$ , beginning in the oxidized, native state. Chemical denaturation data with raw absorbance values and linear

extrapolation fits are shown in Supplementary Figure S5. Qualitatively, the chemical denaturation experiments support trends observed by thermal denaturation. *Fc* cyt  $c_6$  unfolds at lower concentrations of denaturant ( $C_{1/2}$ ) than *Tp* cyt  $c_6$ .

Single-wavelength unfolding curves were fit using the linear-extrapolation method, yielding the free energy change upon unfolding in water ( $\Delta G_{N-D}$ ), and the  $m$ -value, or steepness of the transition (Table 3) [25, 26]. The free energies of unfolding for *Fc* and *Tp* cyt  $c_6$  are the same, within the error of the experiment. However, there is a significant difference in the cooperativity of the unfolding transition; the  $m$ -value for unfolding of *Fc* cyt  $c_6$  is twice the  $m$ -value for unfolding of *Tp* cyt  $c_6$ .

### Midpoint potential and thermal denaturation of reciprocal mutants of *Tp* cyt $c_6$

To identify the role of key amino acid substitutions in modifying the reduction potential and melting temperature of the cytochrome  $c_6$  fold, we generated sequence variants of *Tp* cyt  $c_6$  where single alanine residues were converted to serine residues as observed in homologous positions in the *Fc* cyt  $c_6$  sequence (Fig. 1).

Substituting serine for alanine in *Tp* cyt  $c_6$  caused shifts in the midpoint potential of the heme group but only for

**Table 1** Average midpoint potentials measured for wild-type cytochrome  $c_6$  proteins from *T. pseudonana* and *F. cylindrus* on PGE electrodes at 2 mV/s scan rate

	Midpoint potential (mV vs. SHE)		$\Delta H^\circ_{rc}$ (kJ)	$\Delta S^\circ_{rc}$ (J/K)
	0 °C	15 °C		
<i>Fc</i> cyt $c_6$	383 ± 1	368 ± 1.0	−65.2 ± 0.4	−104 ± 1.5
<i>Tp</i> cyt $c_6$	387 ± 0.6	372 ± 1.7	−63.7 ± 1.7	−96 ± 6
<i>Tp</i> cyt $c_6$ A86S	387 ± 4	374 ± 3		
<i>Tp</i> cyt $c_6$ A93S	380 ± 3	364 ± 3		
<i>Tp</i> cyt $c_6$ A126S	384 ± 4	371 ± 3		
<i>Tp</i> cyt $c_6$ A93S/A126S	376 ± 3	358 ± 2		

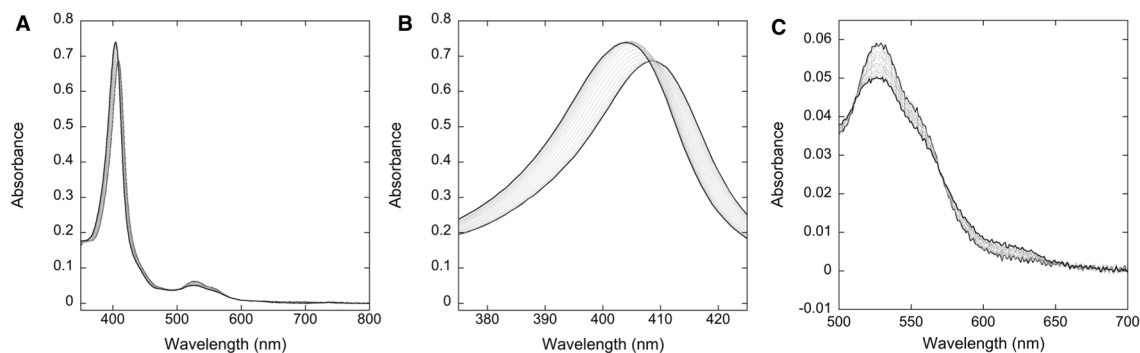


**Fig. 3** UV–Vis spectra collected during thermal unfolding of *Fc* cyt  $c_6$ , showing the full spectra (a), Soret feature only (b) and Q-band region (c). In all cases, the fully folded and fully unfolded endpoints are shown in black, whereas all intermediate temperatures are shown in gray

some of the variants (Table 1). Variants *Tp* cyt *c*<sub>6</sub> A86S and *Tp* cyt *c*<sub>6</sub> A126S showed midpoint potentials within error of the wild-type protein. The *Tp* cyt *c*<sub>6</sub> A93S variant shows a slightly depressed midpoint potential, where the *Tp* cyt *c*<sub>6</sub> A93S/A126S variant shows an even greater decrease in the midpoint potential. Interestingly, the midpoint potentials of both *Tp* cyt *c*<sub>6</sub> A93S and *Tp* cyt *c*<sub>6</sub> A93S/A126S variants are lower than the midpoint potential of *Fc* cyt *c*<sub>6</sub> at equivalent temperatures.

Melting curves generated under oxidizing conditions also showed the position-dependent effects of alanine to serine substitutions (Table 2). While the *Tp* cyt *c*<sub>6</sub> A86S substitution did not cause a significant change in melting temperature, both *Tp* cyt *c*<sub>6</sub> A93S and *Tp* cyt *c*<sub>6</sub> A126S substitutions resulted in an approximately 4 °C drop in melting temperature compared to the wild-type parental construct. The *Tp* cyt *c*<sub>6</sub> A93S/A126S substitution resulted in a 7 °C drop in melting temperature compared to the parental construct.

## Discussion

### Redox properties of diatom cytochrome *c*<sub>6</sub>

Cyclic voltammetry supports the assignment of *Tp*35934 and *Fc*271949 as cytochrome *c*<sub>6</sub>, with typical reduction potentials for the family. A membrane electrode setup allowed measurement of a single, reversible Nernstian process, with a midpoint potential invariant with electrode surface. Midpoint potentials of other cytochrome *c*<sub>6</sub> proteins reported in the literature at 25 °C range from +314 to +358 mV vs SHE [5, 32–35]. When measured at the equivalent temperature of 25 °C, *Fc* cyt *c*<sub>6</sub> and *Tp* cyt *c*<sub>6</sub> midpoint potentials fall on the

**Table 2** Average and standard deviation for triplicate thermal denaturation experiments conducted in 50 mM HEPES pH 7.4

Sample <sup>a</sup>	$T_m$ (K)	$\Delta H_{vH}$ (kJ/mol)
<i>Tp</i> cyt <i>c</i> <sub>6</sub>	312.3 ± 0.8	162 ± 17
<i>Fc</i> cyt <i>c</i> <sub>6</sub>	301.9 ± 0.3	187 ± 7
<i>Tp</i> cyt <i>c</i> <sub>6</sub> A86S	312.0 ± 1.6	183 ± 20
<i>Tp</i> cyt <i>c</i> <sub>6</sub> A93S	308.5 ± 0.7	192 ± 2
<i>Tp</i> cyt <i>c</i> <sub>6</sub> A126S	308.3 ± 0.2	171 ± 32
<i>Tp</i> cyt <i>c</i> <sub>6</sub> A93S/A126S	305.4 ± 0.4	160 ± 4

<sup>a</sup>Experiments were completed in the presence of stoichiometric amounts of potassium ferricyanide oxidizing agent

high end of the range of other known cyt *c*<sub>6</sub>, with values of 355 ± 1.5 mV and 363 ± 1.5 mV vs SHE, respectively.

The psychrophilic cytochrome *c*<sub>6</sub> exhibits redox parameters very similar to the mesophilic homolog. The difference in midpoint potential between *Tp* and *Fc* cyt *c*<sub>6</sub> determined here at 0 °C and 15 °C is very small. Because differences in  $\Delta H^\circ_{rc}$  and  $\Delta S^\circ_{rc}$  between *Tp* and *Fc* cyt *c*<sub>6</sub> are within the error of the experiment, these data suggest that thermodynamic differences in the reduction of *Fc* and *Tp* cyt *c*<sub>6</sub> are subtle, and possibly constrained by evolution. As demonstrated for all other measured *c*-type cytochromes, both  $\Delta H^\circ_{rc}$  and  $\Delta S^\circ_{rc}$  for *Tp* and *Fc* cyt *c*<sub>6</sub> are negative, reflecting that the reduction process is enthalpically favored but entropically disfavored [7, 8]. The only other psychrophilic cytochrome *c* that has been investigated in the literature, *Colwellia psychrerythraea* cytochrome *c*<sub>552</sub>, showed approximate  $\Delta H^\circ_{rc}$  and  $\Delta S^\circ_{rc}$  of −42.5 kJ/mol and −70.3 J/molK, respectively [36]. Both diatom cytochrome *c*<sub>6</sub> proteins investigated here have larger values for  $\Delta H^\circ_{rc}$  and  $\Delta S^\circ_{rc}$  compared to *C. psychrerythraea* cyt *c*<sub>552</sub>, showing that there can be

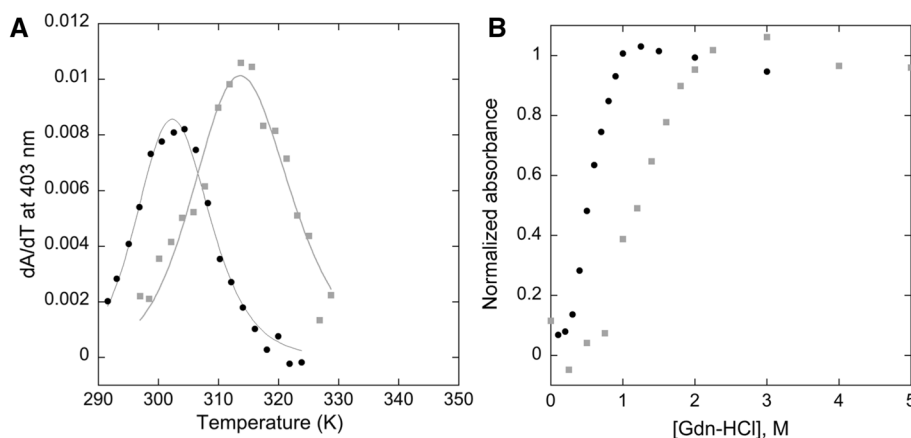


**Fig. 4** Thermal and chemical denaturation of *Fc* and *Tp* cyt *c*<sub>6</sub>. **a** Derivative plots of thermal unfolding of *Fc* cyt *c*<sub>6</sub> (black) and *Tp* cyt *c*<sub>6</sub> (gray). Lines represent the best fits to the derivative form of the van't Hoff equation. **b** Normalized absorbance intensity over increas-

ing concentration of guanidine hydrochloride, [Gdn-HCl], for *Fc* cyt *c*<sub>6</sub> (black) and *Tp* cyt *c*<sub>6</sub> (gray) at 15 °C. Data points represent the average of triplicate measurements, then each curve is normalized to a maximum absorbance of 1 to assist in visual comparison

**Table 3** Linear extrapolation method fits of chemical denaturation data collected at 15 °C

Protein	$\Delta G_{N-D}$ (kJ/mol)	$m$ -value (kJ/mol·M)	$C_{1/2}$
<i>Fc</i> cyt $c_6$	$9.0 \pm 1.1$	$17.0 \pm 1.8$	0.5
<i>Tp</i> cyt $c_6$	$11.0 \pm 2.1$	$9.0 \pm 1.6$	1.2

<sup>a</sup>Experiments included varying concentrations of guanidine hydrochloride in 50 mM HEPES pH 7.4 and 28  $\mu$ M potassium ferricyanide

large differences between psychrophilic  $c$ -type cytochromes, and demonstrating the importance of using close homologs to elucidate mechanisms of thermal adaptation.

### Thermal and chemical denaturation of diatom cytochrome $c_6$

Based on the difference in the optimal growth temperatures for the psychrophile *F. cylindrus* (between 0–10 °C) [14–16] and the mesophile *T. pseudonana* (20–30 °C) [11–13], we hypothesized that there might be a difference in stability of the two cytochrome  $c_6$  proteins. The data demonstrate that the melting temperature of *Fc* cyt  $c_6$  is indeed approximately 10 °C lower than the melting temperature of the mesophilic homolog. While the melting temperature differences are relatively small in magnitude, melting temperatures are all determined with standard deviations of less than 1 °C providing high confidence in the measurements.

The thermodynamic parameters of folding for *Tp* and *Fc* cyt  $c_6$  reported here are in the range of those measured for other red algal and diatom cyt  $c_6$  proteins (Table 4). While the  $m$ -value for *Tp* cyt  $c_6$  is consistent with values measured for red algae and diatom cyt  $c_6$ , the  $m$ -value for the psychrophilic *Fc* cyt  $c_6$  is higher. Therefore, the unfolding of the psychrophilic protein *Fc* cyt  $c_6$  is more cooperative when compared to other measured cytochromes in the  $c_6$  family. This suggests that the larger  $m$ -value may be a specific adaptation to function in a continuously cold environment. Previous studies on alpha-amylases have similarly shown that the chemical denaturation for the enzyme from a psychrophile is more cooperative than those of homologous enzymes from mesophiles, and thermophilic proteins tend to show uncooperative or multistep unfolding [37].

### Effect of alanine to serine substitutions

We generated single-site mutants where alanine positions in *Tp* cyt  $c_6$  sequence were converted to serine. Our data demonstrate that while not all alanine to serine substitutions result in a decrease in melting temperature, alanine to serine substitutions occurring at specific sites decrease the melting temperature by approximately 4 °C. Combining two alanine to serine substitutions into a single wild-type background

results in a melting temperature change of 7 °C. The effect of multiple alanine to serine mutations is approximately additive, but the additive effect falls short of the full 10 °C difference between the wild-type *Fc* and *Tp* cyt  $c_6$  proteins. While alanine to serine substitutions contribute to thermal adaptation, other sequence differences must also be functionally relevant.

To identify why only certain alanine to serine substitutions impacted melting temperature, we used homology modeling to predict the positions of each substitution in the tertiary structure. The Robetta server was used to generate homology models of both *Fc* and *Tp* cyt  $c_6$  sequences using the structure of *Phaeodactylum tricornutum* cyt  $c_6$  [42] (Fig. 5). Notably, none of the mutations are in the heme pocket. Position A86S, which did not result in a change in melting temperature, is located on a solvent exposed, unstructured loop. In contrast, both A93S and A126S positions, which resulted in melting temperature decreases, are fully or partially buried. Solvent accessible surface area calculations predict A93S position to be 1% solvent exposed, whereas A126S position is predicted to be 48% solvent exposed [43]. Therefore, homology modeling suggests that mutations only impact melting temperature if they change the polarity of buried residues.

If alanine versus serine substitutions are also involved in determining the midpoint potential of *Tp* cyt  $c_6$  versus *Fc* cyt  $c_6$ , we expect the serine variants to have lower midpoint potentials than wild-type *Tp* cyt  $c_6$ . Consistent with its position on an unstructured, solvent exposed loop, the A86S variant gave the same midpoint potential as the wild-type parent. While A126S impacted melting temperature, it did not result in a significant decrease in midpoint potential. The A93S variant, located at the most buried of the three positions, showed a small decrease in midpoint potential. Unexpectedly, the A93S/A126S variant showed an even more depressed midpoint potential, reaching a value lower than that of the wild-type *Fc* cyt  $c_6$  at the equivalent temperature. Therefore, alanine to serine substitutions do have small impacts on the midpoint potential, but only at buried positions.

### The role of solvation in cytochrome $c$ adaptation to environmental temperature

In this study, we observe distinct differences in the thermodynamic stability of two closely homologous  $c$ -type cytochromes and show that alanine to serine substitutions contribute to the observed differences. The stability of  $c$ -type cytochromes can be modulated by entropic factors, including changes in solvation, or enthalpic factors. For example, the model system of the mesophilic cytochrome  $c$  from *Pseudomonas aeruginosa* and a thermophilic homolog from *Hydrogenobacter thermophilus* showed that the thermophilic



**Table 4** Free energy of unfolding parameters for oxidized cytochrome  $c_6$  proteins reported in the literature

Protein	$\Delta G_{N-D}$ (kJ/mol)	$m$ -value (kJ/mol·M)	References
<i>Porphyra yezoensis</i> $c_6$ (red algae)	10.1	10.7	[38]
<i>Phaeodactylum tricorutum</i> $c_6$ (diatom)	16.0	10.45	[39]
<i>Nostoc</i> sp. PCC 7119 $c_6$ (cyanobacterium)	21.4	3.6	[40]
<i>Phormidium laminosum</i> $c_6$ (cyanobacterium)	6.5	2.6	[41]
<i>Fc</i> cyt $c_6$ (diatom)	9.0	17.0	This work
<i>Tp</i> cyt $c_6$ (diatom)	11.0	9.0	This work

cyt  $c$  is stabilized primarily through entropic factors [44]. One contributor to the entropic stabilization is the greater mobility and solvent exposure of a glutamine residue in the heme binding pocket of the thermophilic cyt  $c$  [45]. A variant of the mesophilic *P. aeruginosa* cyt  $c$  could be stabilized to match the thermophilic homolog with just five reciprocal mutations chosen to increase side chain packing in the protein interior, yet the resulting protein was primarily stabilized by enthalpic factors [44].

Several lines of evidence suggest that differences in solvation play a role in determining thermal stability differences observed between *Tp* and *Fc* cyt  $c_6$ . The evidence includes: (1) the  $m$ -value for the chemical denaturation of psychrophilic cyt  $c_6$  differs from that of the mesophilic homolog (2) mutations that introduce polar groups into buried positions impact melting temperature. Together, these data point to a role for solvation of the native state in modulating the behavior of the two proteins.

The substantially increased  $m$ -value for the psychrophilic *Fc* cyt  $c_6$  reflects a change in the folding related to solvent accessible surface area. Previous studies on mesophilic and thermophilic homologs of RNase H observed that proteins adapted to lower environmental temperatures showed a larger change in solvent accessible surface area upon unfolding [46]. Consistent with the RNase H model system, the larger  $m$ -value for *Fc* cyt  $c_6$  implies greater change in solvent accessibility during unfolding [47]. This change could arise from *Fc* cyt  $c_6$  having a decreased solvent accessible surface area of the folded state or increased solvent accessible surface area of the unfolded state relative to *Tp* cyt  $c_6$ . In the RNase H system, the difference was attributed to less residual structure in the unfolded state of the mesophile compared to the thermophile [46]; further data is required to determine whether changes in the unfolded or folded state drive the difference observed in *Fc* and *Tp* cyt  $c_6$ .

Furthermore, the fact that alanine to serine mutations decrease the stability of the mesophilic protein supports a role for differing solvation in determining the stability of the wild-type proteins. Only alanine/serine positions that were predicted to be buried resulted in changes in stability. Serine and alanine differ greatly in the energetic cost of burial in the protein interior; a buried serine is both conformationally

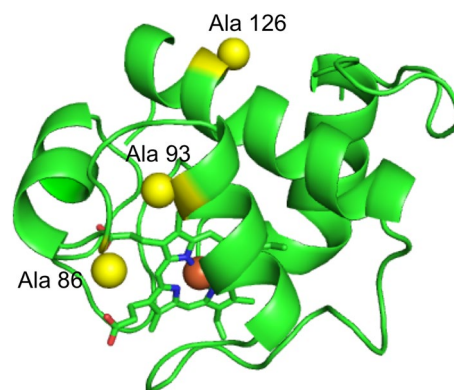


**Fig. 5** Homology model of *Tp* cyt  $c_6$  (PyMOL). Heme group is shown in sticks, and positions of beta carbon atoms of alanine 86, 93 and 126 are shown as yellow spheres

restricted due to hydrogen bonding and more costly to desolvate because of its greater hydrophilicity. The combined conformational restriction and hydrophobicity factors result in a total predicted cost difference for burial of alanine vs. serine of approximately 9 kJ/mol at 300 K [48]. We observe approximately 2 kJ/mol difference between the free energies of unfolding for wild-type *Tp* and *Fc* cyt  $c_6$ , significantly less than the additive cost of burial of two serines instead of alanines. One way to mitigate the cost of burial of serine versus alanine would be an increase in the solvent accessibility of the buried serines of *Fc* cyt  $c_6$ .

Differences in solvation, specifically of the native state, could also explain the modest difference in midpoint potentials of *Fc* and *Tp* cyt  $c_6$ . Solvation has been shown to have a significant impact on the midpoint potential of  $c$ -type cytochromes, but the direction of the change is highly dependent on the location of the solvent molecules. Increased solvent accessibility of the heme group should cause a decrease in midpoint potential due to stabilization of higher charge oxidation states by the relatively polarizable solvent, and this effect has been shown to have a significant effect on tuning heme potentials [49–51]. However, mutations in the heme pocket that increase solvent accessibility can also increase the midpoint potential, perhaps as a result of electrostatic interactions or aromatic hydrogen

bonds formed between the polar group and the porphyrin ring [5]. Increased solvation of a heme propionate has been calculated to raise the standard reduction potential by up to 50 mV [52]. Given the modest 4–10 mV changes in midpoint potentials measured in this study, it is likely that several different compensating effects are at work to minimize the impact of amino acid differences on the potential.

The reduction and unfolding transitions of *c*-type cytochromes are related by a thermodynamic cycle. Changes in reduction potential could be due to changes in stability of the ferrous state, ferric state, or both. In this study, we compare the stabilities of the ferric cytochromes only. Therefore, it is possible that the alanine to serine mutations generated in this study modulate the reduction potentials through changing the stability of the ferrous state.

### Possible compensatory roles for other amino acid differences

Additional varying positions may serve to compensate for the effect of the alanine versus serine substitutions analyzed in this study. The serine (*Fc* cyt *c*<sub>6</sub>) versus asparagine (*Tp* cyt *c*<sub>6</sub>) substitution at position 90 may act to compensate for the alanine versus serine substitution at position 93. *Fc* Ser 90 is predicted based on homology modeling to form a hydrogen bonding network with the side chain of Ser 93 and the backbone carbonyl of Gly 88, forming a stabilizing turn motif between that caps the N-terminal end of the third helix. In *Tp* cyt *c*<sub>6</sub>, position 93 is occupied by alanine, but the longer Asn at position 90 is predicted to form a direct hydrogen bond with the backbone carbonyl of Gly 87, maintaining the helical capping motif. The alanine versus serine substitution at position 128 may serve to mitigate the *Fc* Ser 126 versus *Tp* Ala 126 substitution. As position 126 and 128 occur on the same alpha helix, the *Fc* Ala 128 versus *Tp* Ser 128 ensures one of the two positions in the helix remains alanine, perhaps to maintain helical propensity. Alternatively, because position 128 is entirely buried in the hydrophobic core of the protein, burial of the alanine in *Fc* cyt *c*<sub>6</sub> may contribute a compensatory stabilization to the free energy of folding through greater hydrophobicity and lesser change in conformational entropy.

Another intriguing difference between *Tp* and *Fc* cyt *c*<sub>6</sub> sequences is the additional glutamate residue on the C-terminus of the *Fc* cyt *c*<sub>6</sub> sequence (Fig. 1). The single C-terminal glutamate in *P. tricornutum* cyt *c*<sub>6</sub> is absent from the PDB file and presumably unstructured. However, homology models suggest possible interactions between acidic C-terminal residues and the omega loop immediately following helix I' in the structure in both *Fc* and *Tp* cyt *c*<sub>6</sub>. The additional C-terminal glutamate may have indirect effects on the heme through modifying the structure of

the omega loop and its contacts with the heme propionates. Direct electrostatic effects are unlikely given the predicted 15 Å distance between the C-terminus and the heme iron.

### Conclusions

The folding and reduction of *c*-type cytochromes are thermodynamically coupled phenomena. The data presented here suggest a mechanism where solvation of the folded state is important in adaptation of an electron transfer protein to varying functional temperatures. Increased solvent accessibility of the hydrophobic core is expected to lower the thermodynamic stability and also affect the reduction potential of the heme iron. While a decrease in folding stability would be correlated to greater conformational flexibility at lower temperatures, the functional role of the decreased reduction potential for the psychrophilic protein is less clear. We look forward to future studies comparing psychrophilic and mesophilic electron transfer proteins to understand whether solvation is a common theme in adaptation of redox-active proteins to function at low temperatures.

**Acknowledgements** The authors thank the M. J. Murdock Charitable Trust for funding through the Murdock College Research Program for Natural Sciences. We thank the Seattle University College of Science and Engineering for summer support. Seattle University students enrolled in CHEM 1910 collected key preliminary cyclic voltammetry data for this study.

**Funding** This study was funded by the M. J. Murdock Charitable Trust Murdock College Research Program for Natural Sciences (2015302:MNL).

### Compliance with ethical standards

**Conflict of interest** The authors declare that they have no conflict of interest.

### References

1. Struvay C, Feller G (2012) Optimization to low temperature activity in psychrophilic enzymes. *Int J Mol Sci* 13:11643–11665. <https://doi.org/10.3390/ijms130911643>
2. Casanueva A, Tuffin M, Cary C, Cowan DA (2010) Molecular adaptations to psychrophily: the impact of “omic” technologies. *Trends Microbiol* 18:374–381. <https://doi.org/10.1016/j.tim.2010.05.002>
3. Gianese G, Bossa F, Pascarella S (2002) Comparative structural analysis of psychrophilic and meso- and thermophilic enzymes. *Proteins Struct Funct Genet* 47:236–249. <https://doi.org/10.1002/prot.10084>
4. Marcus RA, Sutin N (1985) Electron transfers in chemistry and biology. *BBA Rev Bioenerg* 811:265–322. [https://doi.org/10.1016/0304-4173\(85\)90014-X](https://doi.org/10.1016/0304-4173(85)90014-X)

5. Worrall JAR, Schlarb-Ridley BG, Reda T et al (2007) Modulation of heme redox potential in the cytochrome  $c_6$  family. *J Am Chem Soc* 129:9468–9475. <https://doi.org/10.1021/ja072346g>
6. Schnackenberg J, Than M, Mann K et al (1999) Amino acid sequence, crystallization and structure determination of reduced and oxidized cytochrome  $c_6$  from the green alga *Scenedesmus obliquus*. *J Mol Biol* 290:1019–1030
7. Battistuzzi G, Borsari M, Sola M, Francia F (1997) Redox thermodynamics of the native and alkaline forms of eukaryotic and bacterial class I cytochromes  $c$ . *Biochemistry* 36:16247–16258. <https://doi.org/10.1021/bi971535g>
8. Terui N, Tachiiri N, Matsuo H et al (2003) Relationship between redox function and protein stability of cytochromes  $c$ . *J Am Chem Soc* 125:13650–13651. <https://doi.org/10.1021/ja035682f>
9. Armbrust EV, Berges JA, Bowler C et al (2004) The genome of the diatom *Thalassiosira pseudonana*: ecology, evolution, and metabolism. *Science* 306:79–86. <https://doi.org/10.1126/science.1101156>
10. Mock T, Otililar RP, Strauss J et al (2017) Evolutionary genomics of the cold-adapted diatom *Fragilariopsis cylindrus*. *Nature* 541:536–540. <https://doi.org/10.1038/nature20803>
11. Berges JA, Varela DE, Harrison PJ (2002) Effects of temperature on growth rate, cell composition and nitrogen metabolism in the marine diatom *Thalassiosira pseudonana* (*Bacillariophyceae*). *Mar Ecol Prog Ser* 225:139–146. <https://doi.org/10.3354/meps225139>
12. Baek SH, Jung SW, Shin K (2011) Effects of temperature and salinity on growth of *Thalassiosira pseudonana* (*Bacillariophyceae*) isolated from ballast water. *J Freshw Ecol* 26:547–552. <https://doi.org/10.1080/02705060.2011.582696>
13. Ferguson RL, Collier A, Meete DA (1976) Growth response of *Thalassiosira pseudonana* Hasle and Heimdal Clone 3H to illumination temperature and nitrogen source. *Chesap Sci* 17:148–158
14. Lizotte MP (2001) The contributions of sea ice algae to antarctic marine primary production. *Am Zool* 41:57–73. [https://doi.org/10.1668/0003-1569\(2001\)041\[0057:TCOSIA\]2.0.CO;2](https://doi.org/10.1668/0003-1569(2001)041[0057:TCOSIA]2.0.CO;2)
15. Lyon BR, Mock T (2014) Polar microalgae: new approaches towards understanding adaptations to an extreme and changing environment. *Biology (Basel)* 3:56–80. <https://doi.org/10.3390/biology3010056>
16. Mock T, Valentin K (2004) Photosynthesis and cold acclimation: Molecular evidence from a polar diatom. *J Phycol* 40:732–741. <https://doi.org/10.1111/j.1529-8817.2004.03224.x>
17. Kilian O, Kroth PG (2005) Identification and characterization of a new conserved motif within the presequence of proteins targeted into complex diatom plastids. *Plant J* 41:175–183. <https://doi.org/10.1111/j.1365-3113X.2004.02294.x>
18. Gruber A, Rocap G, Kroth PG et al (2015) Plastid proteome prediction for diatoms and other algae with secondary plastids of the red lineage. *Plant J* 81:519–528. <https://doi.org/10.1111/tpj.12734>
19. Nordberg H, Cantor M, Dusheyko S et al (2014) The genome portal of the Department of Energy Joint Genome Institute: 2014 updates. *Nucleic Acids Res* 42:D26–31. <https://doi.org/10.1093/nar/gkt1069>
20. Dyrlov Bendtsen J, Nielsen H, von Heijne G, Brunak S (2004) Improved prediction of signal peptides: SignalP 3.0. *J Mol Biol* 340:783–795. <https://doi.org/10.1016/J.JMB.2004.05.028>
21. Arslan E, Schulz H, Zufferey R et al (1998) Overproduction of the *Bradyrhizobium japonicum*  $c$ -type cytochrome subunits of the  $cbb_3$  oxidase in *Escherichia coli*. *Biochem Biophys Res Commun* 247:744–747
22. Berry EA, Trumpower BL (1987) Simultaneous determination of hemes  $a$ ,  $b$  and  $c$  from pyridine hemochrome spectra. *Anal Biochem* 161:1–15
23. Fourmond V (2016) QSoas: a versatile software for data analysis. *Anal Chem* 88:5050–5052. <https://doi.org/10.1021/acs.analchem.6b00224>
24. John DM, Weeks KM (2000) van't Hoff enthalpies without baselines. *Protein Sci* 9:1416–1419. <https://doi.org/10.1110/ps.9.7.1416>
25. Santoro MM, Bolen DW (1988) Unfolding free energy changes determined by the linear extrapolation method. 1. Unfolding of phenylmethanesulfonyl alpha-chymotrypsin using different denaturants. *Biochemistry* 27:8063–8068. <https://doi.org/10.1021/bi00421a014>
26. Knapp JA, Pace CN (1974) Guanidine hydrochloride and acid denaturation of horse, cow, and *Candida krusei* cytochromes  $c$ . *Biochemistry* 13:1289–1294
27. Lojou É, Bianco P (2004) Membrane electrodes for protein and enzyme electrochemistry. *Electroanalysis* 16:1113–1121. <https://doi.org/10.1002/elan.200403001>
28. Correia dos Santos MM, Paes de Sousa PM, Simões Gonçalves ML et al (2003) Electrochemical studies on small electron transfer proteins using membrane electrodes. *J Electroanal Chem* 541:153–162. [https://doi.org/10.1016/S0022-0728\(02\)01427-4](https://doi.org/10.1016/S0022-0728(02)01427-4)
29. Ye T, Kaur R, Senguen FT et al (2008) Methionine ligand lability of type I cytochromes  $c$ : detection of ligand loss using protein film voltammetry. *J Am Chem Soc* 130:6682–6683. <https://doi.org/10.1021/ja801071n>
30. Levin BD, Can M, Bowman SEJ et al (2011) Methionine ligand lability in monoheme cytochromes  $c$ : an electrochemical study. *J Phys Chem B* 115:11718–11726
31. Pettigrew GW, Moore GR (1987) Cytochromes  $c$ : biological aspects. Springer, Berlin
32. Cho YS, Wang QJ, Krogmann D, Whitmarsh J (1999) Extinction coefficients and midpoint potentials of cytochrome  $c_6$  from the cyanobacteria *Arthrospira maxima*, *Microcystis aeruginosa*, and *Synechocystis* 6803. *Biochim Biophys Acta Bioenerg* 1413:92–97. [https://doi.org/10.1016/S0005-2736\(99\)00124-8](https://doi.org/10.1016/S0005-2736(99)00124-8)
33. Bialek W, Nelson M, Tamiola K et al (2008) Deeply branching  $c_6$ -like cytochromes of cyanobacteria. *Biochemistry* 47:5515–5522. <https://doi.org/10.1021/bi701973g>
34. Campos AP, Aguiar AP, Hervas M et al (1993) Cytochrome  $c_6$  from *Monoraphidium braunii*: a cytochrome with an unusual heme axial coordination. *Eur J Biochem* 216:329–341. <https://doi.org/10.1111/j.1432-1033.1993.tb18150.x>
35. Dikiy A, Carpentier W, Vandenberghe I et al (2002) Structural basis for the molecular properties of cytochrome  $c_6$ . *Biochemistry* 41:14689–14699
36. Sokolovskaya OM, Magyar JS, Buzzeo MC (2014) Electrochemical behavior of cytochrome  $c_{552}$  from a psychrophilic microorganism. *J Phys Chem C* 118:18829–18835. <https://doi.org/10.1021/jp501146e>
37. D'Amico S, Marx JC, Gerday C, Feller G (2003) Activity-stability relationships in extremophilic enzymes. *J Biol Chem* 278:7891–7896. <https://doi.org/10.1074/jbc.M212508200>
38. Satoh T, Itoga A, Isogai Y et al (2002) Increasing the conformational stability by replacement of heme axial ligand in  $c$ -type cytochrome. *FEBS Lett* 531:543–547. [https://doi.org/10.1016/S0014-5793\(02\)03615-3](https://doi.org/10.1016/S0014-5793(02)03615-3)
39. Akazaki H, Kawai F, Chida H et al (2008) Cloning, expression and purification of cytochrome  $c_6$  from the brown alga *Hizikia fusiformis* and complete X-ray diffraction analysis of the structure. *Acta Crystallogr Sect F Struct Biol Cryst Commun* 64:674–680. <https://doi.org/10.1107/S1744309108017752>
40. Lange C, Luque I, Hervás M et al (2005) Role of the surface charges D72 and K8 in the function and structural stability of the cytochrome  $c_6$  from *Nostoc sp.* PCC 7119. *FEBS J* 272:3317–3327. <https://doi.org/10.1111/j.1742-4658.2005.04747.x>

41. Mason JM, Bendall DS, Howe CJ, Worrall JAR (2012) The role of a disulfide bridge in the stability and folding kinetics of *Arabidopsis thaliana* cytochrome  $c_{6A}$ . *Biochim Biophys Acta Proteins Proteom* 1824:311–318. <https://doi.org/10.1016/j.bbapa.2011.10.015>
42. Kim DE, Chivian D, Baker D (2004) Protein structure prediction and analysis using the Robetta server. *Nucleic Acids Res.* <https://doi.org/10.1093/nar/gkh468>
43. Fraczkiewicz R, Braun W (1998) Exact and efficient analytical calculation of the accessible surface areas and their gradients for macromolecules. *J Comput Chem* 19:319–333
44. Hasegawa J, Uchiyama S, Tanimoto Y et al (2000) Selected mutations in a mesophilic cytochrome  $c$  confer the stability of a thermophilic counterpart. *J Biol Chem* 275:37824–37828. <https://doi.org/10.1074/jbc.M005861200>
45. Wen X, Patel KM, Russell BS, Bren KL (2007) Effects of heme pocket structure and mobility on cytochrome  $c$  stability. *Biochemistry* 46:2537–2544. <https://doi.org/10.1021/bi602380v>
46. Ratcliff K, Corn J, Marqusee S (2009) Structure, stability, and folding of ribonuclease H1 from the moderately thermophilic *Chlorobium tepidum*: comparison with thermophilic and mesophilic homologues. *Biochemistry* 48:5890–5898. <https://doi.org/10.1021/bi900305p>
47. Myers JK, Nick Pace C, Martin Scholtz J (1995) Denaturant  $m$  values and heat capacity changes: relation to changes in accessible surface areas of protein unfolding. *Protein Sci* 4:2138–2148. <https://doi.org/10.1002/pro.5560041020>
48. Pickett SD, Sternberg MJE (1993) Empirical scale of side-chain conformational entropy in protein folding. *J Mol Biol* 231:825–839. <https://doi.org/10.1006/jmbi.1993.1329>
49. Hosseinzadeh P, Lu Y (2016) Design and fine-tuning redox potentials of metalloproteins involved in electron transfer in bioenergetics. *Biochim Biophys Acta Bioenerg* 1857:557–581. <https://doi.org/10.1016/j.bbabi.2015.08.006>
50. Fantuzzi A, Sadeghi S, Valetti F et al (2002) Tuning the reduction potential of engineered cytochrome  $c$ -553. *Biochemistry* 41:8718–8724. <https://doi.org/10.1021/bi025759x>
51. Tezcan FA, Winkler JR, Gray HB (1998) Effects of ligation and folding on reduction potentials of heme proteins. *J Am Chem Soc* 120:13383–13388. <https://doi.org/10.1021/ja982536e>
52. Bortolotti CA, Amadei A, Aschi M et al (2012) The reversible opening of water channels in cytochrome  $c$  modulates the heme iron reduction potential. *J Am Chem Soc* 134:13670–13678. <https://doi.org/10.1021/ja3030356>

**Publisher's Note** Springer Nature remains neutral with regard to jurisdictional claims in published maps and institutional affiliations.